Development and Preliminary Validation of a Thermally Controlled Modular V-Bending Device: Effect of Punch Radius on ZE10A Magnesium Alloy Sheet

Magali Gallard de Lima[1], Eduardo Luis Schneider[1,*], Leonardo Laranzini[2], Diego Tolotti de Almeida[3], Angelica Paola Oliveira[4] and Deocleber Jorge Radke Padilha[5]

[1]Programa de Pós-Graduação em Engenharia de Minas, Metalúrgica e de Materiais - PPGE3M, Universidade Federal do Rio Grande do Sul - UFRGS, Av. Bento Gonçalves, 9500, Porto Alegre, RS, Brasil

[2]Analista Sênior de Pesquisa Desenvolvimento e Inovação na Bruning Tecnometal – Panambi, Rio Grande do Sul, Brasil

[3]Supervisor de P&D na Bruning Tecnometal Panambi, Rio Grande do Sul e mestrado e doutorado no Programa de Pós-Graduação em Engenharia de Minas, Metalúrgica e de Materiais - PPGE3M, Universidade Federal do Rio Grande do Sul - UFRGS, Porto Alegre, RS, Brasil

[4]Analista de Pesquisa na Bruning Tecnometal Panambi, Rio Grande do Sul e mestrado no Programa de Pós-Graduação em Engenharia Mecânica – PGMEC, Universidade Federal de Santa Maria, UFSM, Santa Maria, RS, Brasil

[5]Técnico de pesquisas e desenvolvimento na Bruning Tecnometal Panambi, Rio Grande do Sul, Brasil

Abstract: The assessment of the formability of magnesium alloy sheets requires testing devices capable of controlling geometric and thermal parameters, since small variations in the bending radius may significantly affect the occurrence of surface cracks. The aim of this work was to develop and preliminarily validate a modular device for V-bending tests with different punch radii, enabling the comparative evaluation of sheet-metal formability. The system was designed to be coupled to a universal testing machine and allows punch replacement while maintaining controlled conditions of temperature, displacement rate, and specimen positioning. As a case study, bending tests were carried out on ZE10A magnesium alloy sheet, commercially known as Elektron® 717, with a nominal thickness of 1.40 mm, at a nominal tool temperature of 175 °C and a soaking time of 20 s. Punch radii of 0.5, 1.0, and 1.5 mm were evaluated, corresponding to approximate R/t ratios of 0.36, 0.71, and 1.07, respectively. Surface damage was quantified by macroscopic inspection and image analysis using ImageJ software, considering the total visible-crack length and its normalized value relative to specimen width. A progressive reduction in surface damage was observed with increasing punch radius. For the 0.5 mm radius, the normalized total visible-crack length reached 84.06% of the specimen width, whereas the 1.0 mm radius resulted in 58.76%. For the 1.5 mm radius, no visible surface cracks were observed under the evaluated condition. Therefore, the device was shown to be sensitive to variations in the geometric severity of bending and suitable as an experimental platform for future studies involving different processing conditions, cutting orientations, and complementary microstructural analyses. One-way analysis of variance confirmed a significant effect of punch radius on the normalized crack-length response ($p < 0.001$). Although validated using ZE10A, the modular architecture is potentially adaptable to comparative testing of other metallic sheet materials.

Keywords: V-bending, Modular device, Punch radius, ZE10A alloy, Magnesium, Formability.

1. INTRODUCTION

Magnesium alloys have attracted increasing interest for lightweight structural applications due to their low density and high specific strength, especially in transportation, mobility, and thin-sheet components. However, the industrial application of magnesium alloy sheets is still limited by their poor room-temperature formability, which is associated with their hexagonal close-packed (HCP) crystal structure, the limited number of easily activated slip systems, and the strong influence of crystallographic texture on mechanical anisotropy [1, 2]. In classical studies on AZ31 sheets, Chen and Huang showed that stamping formability is limited at room temperature but improves significantly with increasing temperature, with a simultaneous reduction in springback and changes in the practical forming limits [1]. The relationship between texture, anisotropy, and mechanical behavior in hexagonal materials was also discussed by Wang and Huang, who highlighted the importance of pole figures, orientation distribution functions, and deformation mechanisms in HCP materials [2].

In magnesium alloys, plastic deformation cannot be interpreted solely in terms of basal slip, especially when loading involves the c-axis direction. In such cases, mechanical twinning plays a fundamental role in accommodating deformation, promoting asymmetric yielding, and controlling microstructural evolution during bending [3]. Barnett *et al*. showed that twin nucleation and growth in magnesium alloys are strongly influenced by grain orientation and Schmid

*Address correspondence to this author at the Programa de Pós-Graduação em Engenharia de Minas, Metalúrgica e de Materiais - PPGE3M, Universidade Federal do Rio Grande do Sul - UFRGS, Av. Bento Gonçalves, 9500, Porto Alegre, RS, Brasil; E-mail: prof.eduardo@ufrgs.br

Received on 08-07-2026 Accepted on 06-08-2026 Published on 10-08-2026

E-ISSN: 2410-4701/26

factor, indicating that the local response to deformation depends on the orientation distribution rather than only on the applied macroscopic stress [3]. More recent assessments have emphasized that the contribution of twinning in wrought magnesium alloys depends not only on the applied stress state but also on texture, loading path, and twin–slip interactions, aspects that are particularly relevant under the tensile–compressive strain gradient generated during bending [4]. This feature is particularly relevant in bending tests, in which regions subjected to tension, compression, and strain gradients coexist through the sheet thickness.

In industrial manufacturing, precise control of the ratio between bending radius and sheet thickness (R/t) is a critical challenge, especially in the production of thin-sheet components for the automotive and mobility sectors. The demand for complex geometries and reduced bending radii often conflicts with the limited ductility of magnesium alloys, making the prediction of surface failure an essential requirement for successful forming.

Increasing temperature is one of the most common strategies used to improve the formability of magnesium alloy sheets, since it promotes the activation of non-basal slip systems, reduces flow stress, and may modify the relative contribution of slip, twinning, dynamic recovery, and dynamic recrystallization. Zhang *et al*. investigated the viscoplastic behavior and microstructural evolution of AZ31B and Elektron 717 magnesium alloys under hot-stamping conditions, showing that ductility increases with temperature and strain rate, although Elektron 717 exhibits a response distinct from AZ31B due to the presence of rare-earth elements and partial suppression of dynamic recrystallization [5]. Bohlen *et al*. compared rolled and extruded magnesium alloy sheets, including AZ31, ZE10, and ME21, demonstrating that the processing route directly affects microstructure, texture, and consequently formability [6]. Complementarily, Stutz *et al*. compared the formability of ZE10 and AZ31 sheets with respect to their initial texture, reinforcing that differences in starting texture may directly influence the response of magnesium alloys during forming operations [7].

In this context, the development of magnesium alloys with weakened texture and improved formability at room or moderate temperatures has become an important research topic. Luo *et al*. reviewed advances in magnesium she*et al*loy development for room-temperature forming, emphasizing that industrial operations such as stamping, flanging, bending, hemming, and cutting are widely performed at room temperature for steels and aluminum alloys but remain challenging for conventional magnesium alloys [8]. Among the technological alternatives, rare-earth-containing magnesium alloys have been studied due to their ability to modify texture, reduce anisotropy, and improve forming response. ZE10A, commercially known as Elektron® 717, is presented by the manufacturer as a highly formable magnesium sheet suitable for thin panels, skins, and enclosures, with the possibility of room-temperature bending at a 1.5 r/t ratio and warm hemming at relatively low temperatures [9].

Despite this potential, the response of ZE10A under processing windows below the temperatures commonly explored for hot stamping still requires further experimental investigation. Schneider *et al*. investigated the mechanical property evolution of ZE10A subjected to thermomechanical treatments between 250 and 300 °C, showing a reduction in mechanical strength with increasing temperature and evidence of incipient dynamic recovery/recrystallization in this temperature range [10]. These results reinforce the relevance of investigating intermediate or moderate heating conditions, in which formability may be improved without necessarily relying on very high temperatures.

In addition to temperature, the forming mode and tool geometry directly influence stress distribution, outer-fiber strain, springback, and crack formation. Richter *et al*. discussed tempered forming of magnesium alloys using roll forming as an example, highlighting that the forming of magnesium alloy sheets requires process adaptation and integrated thermal control to compensate for their poor cold formability [11]. In another approach related to tool development, Silva *et al*. designed and manufactured tool surfaces with different geometries for tribological testing under temperature-supported forming of AZ31 sheets, demonstrating how changes in tool design can be experimentally evaluated under process-representative conditions [12]. This type of approach is relevant to the present work because it shows that the development of specific devices or tools may constitute a technical contribution when associated with controlled experimental validation.

Bending, in particular, is a simple and widely used operation for evaluating ductility, springback, and susceptibility to crack formation in sheet metals. In addition, parameters such as minimum bending radius and R/t ratio are commonly used as practical indicators of the forming capability of magnesium alloy sheets. Xu *et al*. showed that an AZ31 sheet fabricated by a short-process manufacturing route exhibited high bendability, being bent with a radius of only 0.2 times the sheet thickness in a 90° bending test, without visible cracks or surface defects [13]. Early air-bending experiments on AZ31 magnesium alloy sheets also demonstrated that bendability is strongly dependent on tool geometry, material orientation, and thermal condition [14]. The authors attributed this high bending capability to the combination of refined recrystallized microstructure, low residual strain, and activation of prismatic slip in recrystallized grains [13].

Habibnejad-Korayem *et al*. also demonstrated that microstructural modifications induced by bending–unbending cycles and heat treatment can improve the bendability of AZ31 sheets, highlighting the importance of specific tests for evaluating the response of magnesium alloys to bending [15]. Under V-bending conditions, Wang L. *et al*. investigated the evolution of springback and neutral layer position in AZ31B sheets under warm forming conditions, showing that geometric bending parameters, including punch radius, directly affect the mechanical response of the process [16].

Recent studies have shown that bending tests in magnesium alloys can provide important information on the interaction between tool geometry, temperature, deformation mode, and microstructural response. Wang H. *et al*. combined finite element simulation and experimental U-bending tests in a high-strength Mg-Gd-Y-Zn-Zr alloy, showing that increasing temperature reduces equivalent stress, equivalent strain, and bending force, while experimental validation may show good agreement with simulation [17]. Okayasu *et al*. studied the bending of AZ31 sheets under cold and hot conditions, demonstrating that microstructure, prior deformation, and temperature significantly affect formability and springback [18]. Weiss *et al*. investigated different bending-dominated forming modes in AZ31 sheets, including pure bending, V-bending, channel bending, and roll forming, relating the forming mode to the twinned area fraction and springback [19]. Kuo and Lin evaluated springback in AZ31 sheets during L-bending using the Taguchi method to analyze parameters such as punch radius, die clearance, and tool geometry [20].

Tension–compression asymmetry is also particularly important in bending operations, since the sheet thickness is simultaneously subjected to tensile and compressive stress states. Wang Y. *et al*. showed that tension–compression asymmetry in ZA21 magnesium bars is associated with the differential activation of slip and twinning, as well as with twin variant selection as a function of crystallographic orientation [21]. Rustom *et al*. discussed manufacturing strategies to mitigate deformation twinning in magnesium, emphasizing that excessive twinning may be associated with strain-path anisotropy, local incompatibilities, and reduced ductility [22]. These studies reinforce that bending tests in magnesium should not be interpreted merely as a macroscopic assessment of cracking, but rather as a mechanical condition that is sensitive to texture, specimen orientation, bending radius, and thermal state.

In this sense, the development of specific testing devices has been employed in different areas of mechanical and manufacturing engineering to enable geometric control, repeatability, and experimental validation of procedures not fully covered by conventional commercial configurations. Studies on incremental forming, for example, have demonstrated the importance of devices and experimental strategies capable of controlling tool paths, forces, and material response during localized deformation processes [23, 24]. Dedicated bending devices have also been proposed for special testing conditions, including small-scale systems for in situ testing [25].

From a normative perspective, bending tests for metallic materials are covered by standards such as ASTM E290 and ISO 7438, which establish general principles for evaluating ductility by bending [26,27]. However, in studies involving low-formability materials such as magnesium alloy sheets, the direct application of these procedures may not be sufficient to systematically explore the combined influence of geometric and thermal parameters. In particular, controlled variation of punch radius is relevant because smaller radii increase the strain imposed on the outer fiber of the sheet, promoting crack formation, whereas larger radii tend to reduce the local severity of bending. In this context, the main contribution of this work lies in the integration, in a single modular device, of thermal control and punch interchangeability, allowing the influence of bending radius to be assessed under controlled and reproducible conditions.

Unlike previously reported bending fixtures, which are generally configured for a fixed radius, a specific bending mode, or specialized small-scale in situ testing [16, 20, 25], the present device integrates interchangeable precision-machined punches, active heating of both punch and die, multipoint temperature monitoring, a mechanical end stop, and direct coupling to a conventional universal testing machine. The punch radius can therefore be changed without altering the specimen support, thermal-control architecture, or terminal tool position. The novelty of the system lies in this integrated combination of modular geometry and controlled heating, rather than in the V-bending principle itself.

To address this gap, the present work proposes the development and preliminary validation of a modular device for V-bending tests with different punch radii, applied as a case study to ZE10A magnesium alloy sheet, commercially known as Elektron® 717. The main objective is not to provide a complete metallurgical analysis of the alloy, but to demonstrate the design, construction, and initial application of the device under controlled conditions. For this purpose, punch radii of 0.5, 1.0, and 1.5 mm were compared in tests conducted at 175 °C, with thermal control of the die–punch assembly and macroscopic assessment of surface damage by visual inspection and image analysis. This approach illustrates the sensitivity of the method to the geometric severity of bending while establishing an experimental platform for future studies involving other temperatures, soaking times, cutting orientations, and complementary microstructural analyses.

2. MATERIALS AND METHODS

2.1. Design and Construction of the Testing Device

A modular device was developed for V-bending tests with different punch radii, according to the CAD design shown in Figure **1B**. The device concept was based on the general principles of the V-bending test described in ISO 7438 [27], as schematically illustrated in Figure **1A**, but adapted to allow punch replacement and testing under thermal control.

The device was designed to be coupled to a universal testing machine, allowing controlled punch displacement over rectangular sheet specimens. The main feature of the system is its modularity, enabling the evaluation of different bending radii without changing the overall test configuration. This feature is particularly relevant for low-formability materials, in which small geometric variations can significantly modify bending severity and the tendency for surface crack formation.

2.2. Material and Specimen Preparation

The material used as a case study was a ZE10A magnesium alloy sheet, commercially known as Elektron® 717, with a nominal thickness of 1.40 mm. The specimens were cut from the sheet using the rolling direction (RD) and transverse direction (TD) as references for specimen orientation and positioning. The final specimen geometry and nominal dimensions are shown in Figure **2**.

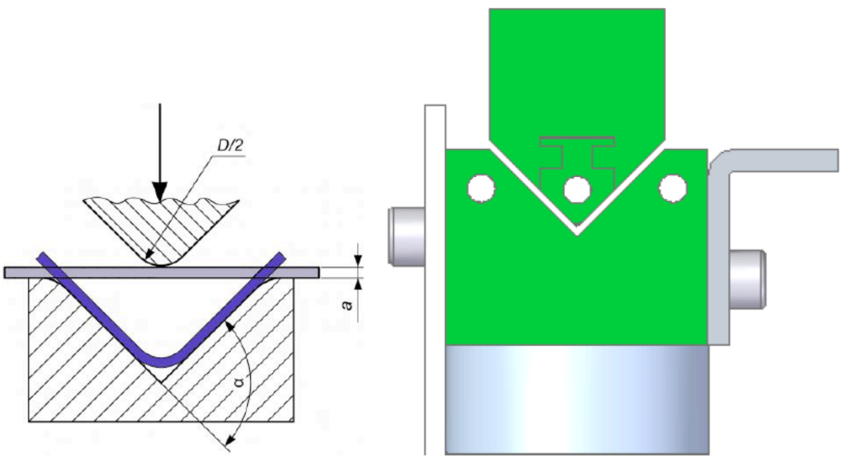

Figure 1: (**A**) Schematic representation of a V-bending test based on the general principles of ISO 7438:2016. (**B**) Device developed for bending tests with different punch radii.

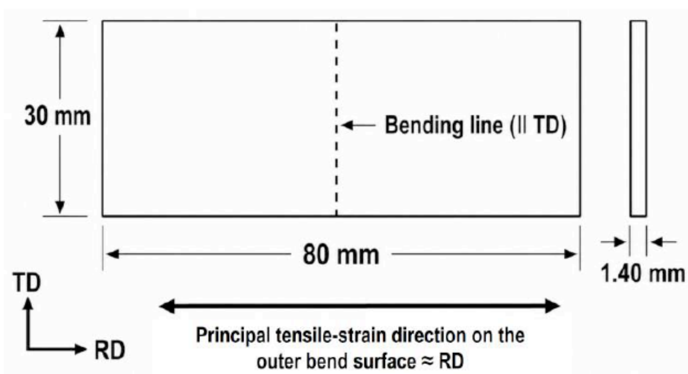

Figure 2: Geometry and nominal dimensions of the ZE10A specimen used in the V-bending tests, indicating the rolling direction (RD), transverse direction (TD), and bend line parallel to TD. Under this configuration, the principal tensile-strain direction on the outer bend surface is approximately parallel to RD.

The specimens used in the bending tests had final dimensions of 80 × 30 × 1.40 mm. The bending line orientation was defined with respect to the rolling direction of the sheet. The preliminary validation presented in this study was restricted to a soaking time of 20 s and a bending line parallel to the transverse direction (TD), which was used to illustrate the sensitivity of the device to punch-radius variation. Under this configuration, the principal tensile-strain direction on the outer bend surface is approximately parallel to the rolling direction (RD).

2.3. Testing Machine and Die–Punch Assembly

The tests were carried out using an EMIC DL-20000 universal testing machine, with a maximum capacity of 200 kN, equipped with TESC 3.04 software. The system allows operation at displacement rates between 0.01 and 500 mm·min^{-1}. In the bending tests, the maximum crosshead speed available in the testing machine, 500 mm·min^{-1}, was selected to reduce heat loss during punch travel and to improve the consistency of the nominal thermal condition. No direct equivalence with industrial press speeds is implied.

The die–punch assembly was manufactured according to the dimensional design shown in Figure **3**. The die has a V-shaped geometry with a nominal opening of 25 mm and an included angle of 90°, allowing adequate positioning of the specimen during testing. Punches with radii of 0.5, 1.0, and 1.5 mm were used, corresponding to approximate R/t ratios of 0.36, 0.71, and 1.07, respectively, considering the nominal sheet thickness of 1.40 mm. These three radii were selected to represent different levels of bending severity, allowing the sensitivity of the device to the geometric variation of the test to be evaluated.

All die and punch components were manufactured on a precision CNC machining center. Fit-related dimensions followed the tolerances specified in the CAD drawings, including 17.000 mm (+0/−0.018), 7.000 mm (+0/−0.015), 5.000 mm (+0.012/0), 2.000 mm (+0/−0.010), and Ø6.6 mm (+0.015/0). For dimensions without an explicit drawing tolerance, conservative manufacturing tolerances of ±0.10 mm for linear dimensions and ±0.5° for angular dimensions were adopted. The nominal punch-tip radii were generated by CNC contour milling. Because no independent post-machining profilometry record was available, a conservative process-based tolerance of ±0.05 mm is assigned to the nominal radii; this value is substantially smaller than the 0.5 mm interval between consecutive punch radii.

2.4. Heating System and Temperature Control

The die–punch assembly was heated using internal electrical heating elements installed in the tooling. Temperature was controlled using a five-zone Polimold digital control system, which provided individual setpoint and feedback display for each active heating zone [29]. Temperature monitoring was performed using calibrated type-K thermocouples, one installed in the punch and two in the die; these thermocouples were the primary quantitative sensors. The nominal thermal condition of the assembly was additionally surveyed by infrared thermography using a Fluke Ti10 camera, as shown in Figure **4**. According to the manufacturer, the Ti10 has a measurement range from −20 to 250 °C, a 160 × 120 detector, a thermal sensitivity of ≤0.2 °C at 30 °C, and an absolute accuracy of ±5 °C or 5%, whichever is greater [28]. Consequently, thermography was used qualitatively to identify marked hot or cold regions and not as the primary measurement of absolute temperature.

Before testing, the assembly was heated until thermal stabilization. A steady-state condition was accepted only when each thermocouple reading remained within ±2 °C of its steady value for 60 s. During the test campaign, the difference among the monitored punch and die positions was maintained

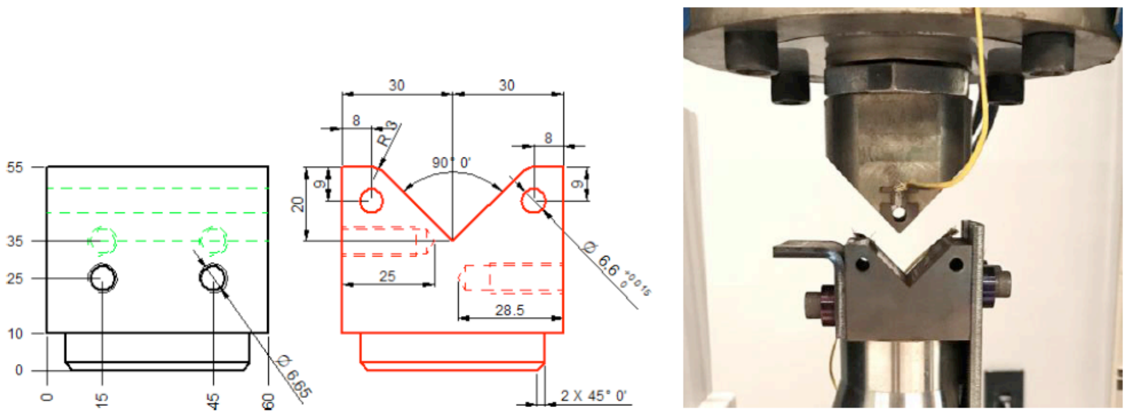

Figure 3: (**a**) Technical drawing of the die with front and side views. (**b**) Die and punch manufactured according to the dimensional design.

within approximately 5 °C before specimen insertion. After stabilization, the specimen was positioned in the device and kept in contact with the heated assembly during the defined soaking time. Because the specimen itself was not instrumented, 175 °C is reported throughout this work as the nominal tool temperature rather than as a directly measured specimen temperature. The die–specimen–punch assembly was wrapped with aluminum foil to reduce heat losses and promote greater temperature homogeneity during testing.

Figure 4: Fluke Ti10 thermographic camera used for thermal monitoring of the die–specimen–punch assembly during testing.

2.5. Experimental Conditions of the Bending Tests

The V-bending tests were conducted at a nominal tool temperature of 175 °C using punch radii of 0.5, 1.0, and 1.5 mm. The selected temperature represents a relatively low warm-forming condition, intentionally below the higher ranges commonly adopted for hot stamping, and was chosen to determine whether the device could distinguish the effect of punch radius under limited thermal assistance. A soaking time of 20 s was selected as an intermediate compromise between tool-to-sheet heat transfer and a short experimental cycle. The bend line parallel to the transverse direction (TD) was selected for this first validation because preliminary trials indicated greater resistance to surface cracking in this orientation, allowing the three punch radii to produce a response ranging from substantial cracking to no visible cracking. Accordingly, the selected matrix was intended to validate the sensitivity of the device and not to establish a complete forming window for ZE10A. The tests were performed without lubrication, and each test was terminated when the punch reached the mechanical end stop of the device. Table **1** summarizes the main parameters controlled during the tests.

The terminology associated with bending direction, R/t ratio, tool geometry, and surface inspection was adopted based on the general principles of ASTM E290 [26] and ISO 7438 [27].

2.6. Macroscopic Inspection and Quantification of Surface Damage

After bending, each specimen was inspected on the outer bend surface, corresponding to the tensile side during testing. The samples were photographed under diffuse lighting, with a calibrated scale positioned in the same plane as the analyzed surface. The images were subsequently evaluated using ImageJ software.

Table 1: Summary of the Parameters Controlled During V-Bending Tests of ZE10A (Elektron® 717)

Parameter	Adopted level / condition	Remarks
Nominal tool temperature (°C)	175	Setpoint controlled in the tool; monitored by thermocouples and Fluke Ti10 thermography
Soaking time (s)	20	Counted after thermal stabilization
Orientation	Bend line ∥ TD	Principal tensile-strain direction on the outer bend surface approximately parallel to RD
Punch radius (mm)	0.5; 1.0; 1.5	R/t ≈ 0.36; 0.71; 1.07
Die opening / included angle	25 mm / 90°	Nominal V-die geometry
Lubrication	None	Tests performed dry
End criterion	Mechanical end stop	Test terminated when the punch reached the mechanical end stop
Replicates	n = 3 per condition	Mean and standard deviation calculated for each condition
Thermal stability criterion	±2 °C for 60 s; ≈5 °C maximum difference among monitored tool positions	Based on calibrated type-K thermocouples before specimen insertion
Punch-radius tolerance (estimated)	±0.05 mm	Conservative process-based estimate for precision CNC contour milling; not independently profiled

Surface damage was quantified by identifying and measuring visible cracks along the bent region. When more than one crack was observed in the same specimen, the individual crack lengths were summed, resulting in the total visible-crack length per specimen. To ensure reproducibility of the analysis, only cracks longer than 0.5 mm were counted, in order to exclude surface roughness or machining marks that could be mistakenly interpreted as structural damage. Scale calibration in ImageJ was repeated for each image using the reference positioned in the same plane as the specimen surface. Based on the specimen width represented in the calibrated images, the spatial scale was approximately 0.05–0.07 mm per pixel; therefore, the 0.5 mm acceptance threshold corresponded to approximately 7–10 pixels. Considering scale calibration and endpoint selection, the uncertainty of an individual crack-length measurement was estimated as approximately ±0.1 mm. All images were analyzed by the same trained operator using the same calibration and tracing procedure, which minimized operator-dependent variation. However, an inter-operator reproducibility study was not performed and is recognized as a limitation. Thus, in this work, the term “total visible-crack length” refers to the sum of the lengths of all visible cracks identified in a given specimen.

In addition to the total visible-crack length, a normalized parameter was calculated according to Eq. (1):

$$L_{norm} = \frac{\sum_{i=1}^{n} L_i}{W} \times 100 \quad (1)$$

where Li is the length of each identified visible crack, n is the number of cracks, and W = 30 mm is the nominal specimen width. As a cumulative normalized length, this parameter does not represent an independent affected area and may theoretically exceed 100% when multiple cracks are present. This parameter is reported as normalized total visible-crack length (% of specimen width). For each experimental condition, the mean and standard deviation of the values obtained from the replicates were calculated.

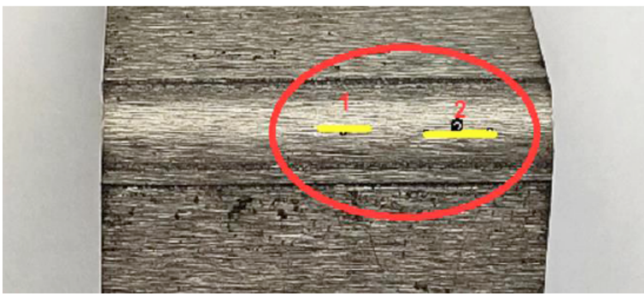

Figure 5: Example of crack number and crack length evaluation in a bent specimen using ImageJ software.

2.7. Statistical Analysis

The normalized total visible-crack length was compared among the three punch radii by one-way analysis of variance (ANOVA), adopting a significance level of α = 0.05. When a significant overall effect was detected, Tukey’s honestly significant difference (HSD) test was used for pairwise comparisons. Because each condition contained only three replicates and the 1.5 mm group exhibited zero within-group variance, a Kruskal–Wallis test was additionally calculated as a non-parametric robustness check. The analyses were performed using the individual specimen values, rather than the reported means.

3. RESULTS

The effect of punch radius on surface damage after bending is presented in Table **2** and illustrated in Figures **6** and **7**. For the test condition at 175 °C, with a soaking time of 20 s and a bending line parallel to the transverse direction (TD), a clear reduction in surface damage was observed with increasing punch radius. The 0.5 mm radius resulted in the highest level of damage, with a mean total visible-crack length of 25.22 ± 2.49 mm and a normalized total visible-crack length of 84.06 ± 8.30% of the specimen width. For the intermediate radius of 1.0 mm, the mean total visible-crack length decreased to 17.63 ± 2.67 mm, corresponding to a normalized total visible-crack length of 58.76 ± 8.90%. For the 1.5 mm radius, no visible surface cracks were observed under the evaluated condition, resulting in 0 mm and 0%, respectively. The standard deviations observed for the 0.5 and 1.0 mm radii indicate moderate variation among replicates, which is compatible with the localized nature of crack nucleation and propagation.

The one-way ANOVA confirmed a statistically significant effect of punch radius on normalized total visible-crack length, $F(2,6) = 113.04$, $p < 0.001$. Tukey HSD comparisons indicated significant differences between 0.5 and 1.0 mm ($p = 0.0107$), 0.5 and 1.5 mm ($p < 0.001$), and 1.0 and 1.5 mm ($p < 0.001$). The Kruskal–Wallis test provided a consistent result ($H = 7.45$, $p = 0.024$). Although these analyses support the observed radius effect, the statistical conclusions should be interpreted as preliminary because n = 3 per condition.

The macroscopic comparison presented in Figure **6** visually confirms this trend. The specimen bent with a 0.5 mm radius showed continuous and distributed cracking along the outer bend surface, whereas the condition with a 1.0 mm radius showed less intense damage. In contrast, the specimen bent with a 1.5 mm radius showed no visible cracks in the analyzed region. Figure **7** summarizes this response, showing the progressive reduction in normalized total visible-crack length with increasing punch radius.

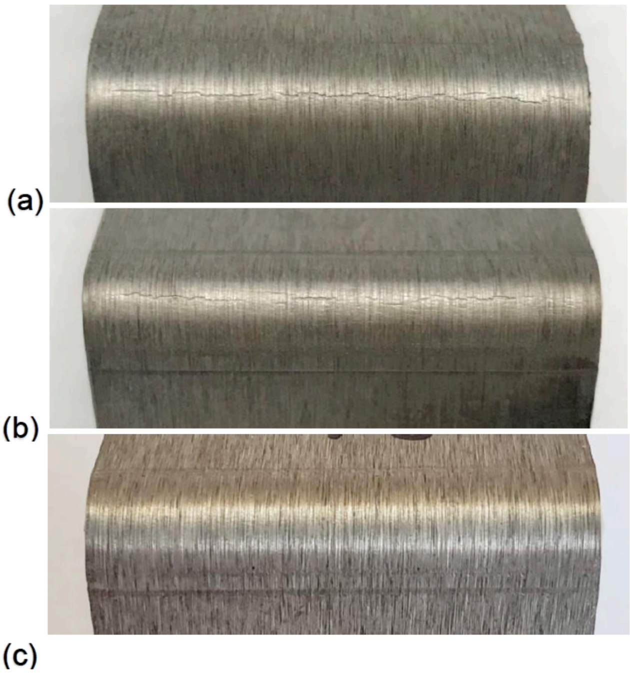

Figure 6: Macroscopic aspect of the outer bend surface of ZE10A specimens bent at 175 °C, with a soaking time of 20 s and bending line parallel to the transverse direction (TD), using punch radii of: (**a**) 0.5 mm, with a normalized total visible-crack length of 84.06% of the specimen width; (**b**) 1.0 mm, with 58.76%; and (**c**) 1.5 mm, without visible surface cracks.

3.1. Discussion of the Results

The results demonstrate that the developed device was able to clearly distinguish the effect of punch radius on the severity of surface damage in bending tests of the ZE10A alloy. The progressive reduction in normalized total visible-crack length, from 84.06% to 58.76% and finally to 0%, when the punch radius increased from 0.5 to 1.0 and 1.5 mm, respectively, demonstrates the sensitivity of the method to the geometric variation imposed by the tooling. This behavior confirms the suitability of the device for comparative formability studies, especially in magnesium alloys, in which small variations in bending conditions can significantly affect the occurrence of surface cracking. The statistical analysis corroborated the macroscopic trend, with all three radii assigned to distinct Tukey groups; the non-parametric test led to the same overall conclusion despite the small sample size.

From a mechanical standpoint, the greater severity observed for the 0.5 mm radius is associated with the increased strain imposed on the outer fiber of the sheet during bending. Considering the nominal thickness of 1.40 mm, the radii of 0.5, 1.0, and 1.5 mm correspond approximately to R/t ratios of 0.36, 0.71, and 1.07, respectively. Thus, the 0.5 mm radius represents a

Table 2: Preliminary Quantification of Surface Damage after V-Bending Tests of ZE10A Alloy at 175 °C, with a Soaking Time of 20 s and Bending Line Parallel to the Transverse Direction (TD), as a Function of Punch Radius

Punch radius (mm)	Total visible-crack length (mm)	Normalized total visible-crack length (% of specimen width)
0.5	25.22 ± 2.49	84.06 ± 8.30 [a]
1.0	17.63 ± 2.67	58.76 ± 8.90 [b]
1.5	0	0 [c]

Note: Different superscript letters indicate statistically significant differences according to Tukey HSD ($p < 0.05$).

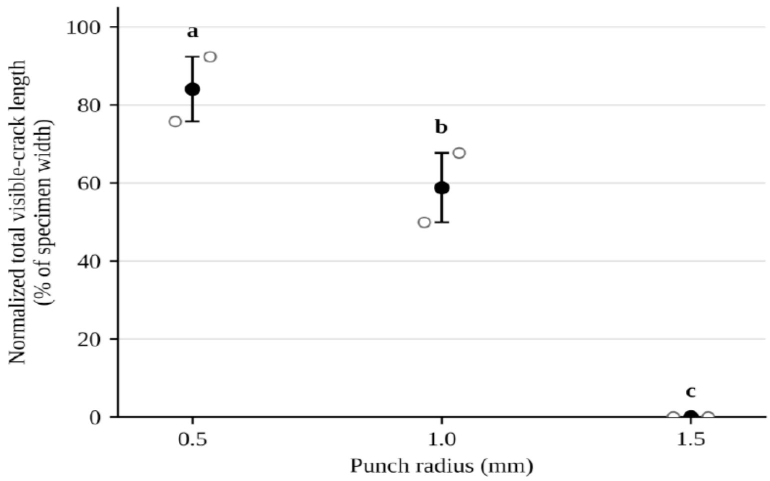

Figure 7: Normalized total visible-crack length as a function of punch radius for ZE10A alloy bent at 175 °C, with a soaking time of 20 s and bend line parallel to TD. Open circles represent individual specimens, filled circles represent the mean, and error bars represent one standard deviation. Different letters indicate statistically significant groups according to Tukey HSD ($p < 0.05$).

severe bending condition, in which the localized deformation on the outer bend surface tends to exceed the plastic accommodation capacity of the material, favoring crack nucleation and propagation. Increasing the radius reduces the imposed curvature and, consequently, the strain on the tensile surface, explaining the reduction in damage observed for 1.0 mm and the absence of visible cracks for 1.5 mm. The standard deviations observed for the 0.5 mm (8.3%) and 1.0 mm (8.9%) radii reflect the inherently stochastic nature of crack nucleation and propagation in magnesium alloys. This variability may be attributed to the influence of local crystallographic texture and grain orientation relative to the stress field, since the activation of deformation mechanisms such as twinning strongly depends on the Schmid factor of each individual grain, as discussed by Barnett *et al*. [3] and further reviewed by Shah *et al*. [4].

This trend agrees with the expected behavior of magnesium alloy sheets, whose formability is limited by the HCP structure and by the dependence of deformation mechanisms on texture, temperature, and stress state. Under bending conditions, the sheet is simultaneously subjected to tension on the outer bend surface and compression on the inner bend surface, making the material response sensitive to tension–compression asymmetry, twinning activation, and local crystallographic orientation. Previous studies indicate that twinning in magnesium depends on grain orientation and Schmid factor [3], while tension–compression asymmetry is related to the differential activation of slip and twinning [21]. Therefore, although the present study is preliminary and macroscopic in nature, the results are consistent with the high sensitivity of magnesium alloys to local deformation conditions.

The absence of visible cracks for the 1.5 mm radius is also consistent with the higher formability attributed to ZE10A/Elektron® 717 compared with conventional magnesium alloys such as AZ31. This result is particularly relevant when contrasted with the behavior of AZ31, which typically shows higher susceptibility to cracking at low or moderate temperatures due to its strong basal texture. The surface integrity maintained in ZE10A for $R/t \approx 1.07$ at 175 °C is consistent with literature reports associating Mg-RE alloys with texture weakening and improved formability, suggesting a more favorable processing window than that normally observed in conventional magnesium alloys subjected to severe geometric conditions. The presence of rare-earth elements in ZE10/Elektron 717 alloys is associated with texture modification and improved formability, although the final response depends on the processing route and thermal condition. Previous studies have shown that the processing route directly affects the texture and formability of AZ31, ZE10, and ME21 alloys [6], and that Elektron 717 exhibits a viscoplastic behavior distinct from AZ31B under hot-stamping conditions [5]. In addition, the manufacturer's datasheet indicates that Elektron® 717 can be bent at room temperature with a 1.5 r/t ratio, reinforcing its potential for applications involving formed sheet components [9]. In the present work, the absence of cracking for $R/t \approx 1.07$ at 175 °C suggests that the combination of a less severe radius and moderate heating was sufficient to avoid visible surface damage under the evaluated condition.

Table 3: Comparison of Representative Bending Studies on Magnesium Alloy Sheets and the Present Work

Study / material	Bending configuration and condition	Main variable(s)	Principal finding
Xu *et al*. [13] / AZ31	90° bending of short-process sheet	R/t = 0.2	No visible cracks; high bendability associated with a refined recrystallized microstructure and activation of additional slip modes.
Paisarn *et al*. [14] / AZ31	Air bending under different processing conditions	Tool geometry, orientation, and thermal condition	Bendability was strongly dependent on the combined geometric, material-orientation, and thermal parameters.
Wang L. *et al*. [16] / AZ31B	Warm V-bending	Punch radius and thermal condition	Punch radius influenced springback and the position of the neutral layer.
Wang H. *et al*. [17] / Mg–Gd–Y–Zn–Zr	Experimental and simulated U-bending at elevated temperature	Temperature	Increasing temperature reduced equivalent stress, equivalent strain, and bending force.
Okayasu *et al*. [18] / AZ31	Cold and hot bending after different prior treatments	Microstructure, prior deformation, and temperature	Formability and springback were strongly modified by the initial condition and test temperature.
Weiss *et al*. [19] / AZ31	Pure, V-, channel, and roll bending	Bending mode	The forming mode altered the twinned area fraction and springback response.
Present study / ZE10A	V-bending at 175 °C; 20 s; bend line ∥ TD	R/t = 0.36, 0.71, and 1.07	Normalized visible-crack length decreased from 84.06% to 58.76% and 0%; the radius effect was statistically significant ($p < 0.001$).

A focused comparison with previously published bending studies is presented in Table **3**. The present results are consistent with the general observation that bending response is highly sensitive to tool geometry, temperature, material texture, and forming mode [13, 14, 16-19]. In warm V-bending of AZ31B, punch radius was reported to affect springback and neutral-layer evolution [16], whereas U-bending investigations of a high-strength Mg–Gd–Y–Zn–Zr alloy showed that increasing temperature reduced equivalent stress, strain, and bending force [17]. Studies involving AZ31 also demonstrated that prior microstructure and thermal condition affect formability and springback [18], and that different bending modes modify the twinned area fraction and elastic recovery [19].

Direct numerical comparison among these studies must remain qualitative because sheet thickness, texture, alloy condition, bend angle, temperature, and damage criteria differ. Nevertheless, the absence of visible cracking for commercial ZE10A at R/t ≈ 1.07 and 175 °C is compatible with the improved formability commonly reported for rare-earth-containing magnesium sheets, while the clear deterioration at smaller radii confirms that tool geometry remains a dominant process variable.

The main advance of this work is the demonstration that the developed device allows controlled bending conditions to be applied and different levels of geometric severity to be distinguished. The inclusion of three punch radii in the TD condition showed that the setup is sensitive to radius variation and suitable for identifying preliminary formability windows. This result supports the use of the device as an experimental platform for future studies involving other temperatures, soaking times, cutting orientations, and complementary microstructural characterizations, such as optical microscopy, SEM, EBSD, or texture analysis. From an engineering perspective, the device provides a practical means of screening punch-radius limits under a controlled thermal state before undertaking more extensive forming campaigns or numerical-model calibration.

The present experimental matrix was intentionally restricted to one temperature, one soaking time, and one material orientation because the primary objective was to validate the sensitivity and repeatability of the device rather than to construct a complete ZE10A forming map. Consequently, the results cannot be generalized to other temperatures, dwell times, orientations, or loading rates without additional testing. The temperature of 175 °C represents a low warm-forming condition, the 20 s soaking time represents an intermediate transfer period, and the selected TD bend-line configuration was chosen because it provided a response range that included both extensive cracking and a crack-free condition.

The current evaluation is also limited to macroscopic surface inspection. Optical microscopy and SEM of the outer bend surface and cross-section will be used in future work to characterize crack initiation and propagation, while EBSD will be applied to quantify texture, twinning, and local orientation effects. Systematic force–displacement acquisition will also be incorporated in the next test campaign; the original files for the specific preliminary specimens evaluated here could not be recovered with sufficient confidence for inclusion. Additional planned work includes direct specimen-temperature measurement, post-machining profilometry of the punch radii, inter-operator repeatability assessment for ImageJ measurements, and broader matrices involving temperature, soaking time, RD/TD orientation, and other sheet materials.

4. CONCLUSIONS

Based on the development of the device and the preliminary bending tests carried out on the ZE10A alloy, the following conclusions can be drawn:

1. A modular device for V-bending tests was developed and built, allowing the use of different punch radii and coupling to a universal testing machine. The system proved suitable for conducting controlled tests on metallic sheets.

2. The device allowed the punch radius to be varied while keeping the main test parameters constant, including temperature, soaking time, displacement rate, and specimen orientation. This feature confirms its applicability in comparative formability studies.

3. In the preliminary tests performed on ZE10A alloy at 175 °C, with a soaking time of 20 s and bending line parallel to the transverse direction (TD), a progressive reduction in surface damage was observed with increasing punch radius.

4. The condition with a punch radius of 0.5 mm showed the highest level of surface damage, with a normalized total visible-crack length of 84.06% of the specimen width, whereas the 1.0 mm radius resulted in 58.76%. For the 1.5 mm radius, no visible surface cracks were observed under the evaluated condition.

5. The engineering significance of the device lies in its ability to screen the influence of punch radius under controlled warm-forming conditions, supporting tool selection and reducing

trial-and-error before larger forming campaigns or numerical simulations.

6. Although experimentally validated using ZE10A, the interchangeable punch system, mechanical end stop, and thermal-control architecture can be adapted to comparative testing of aluminum, steel, titanium, and other metallic sheet materials, provided that the temperature range, tool geometry, and machine capacity are appropriate.

ACKNOWLEDGMENTS

The authors acknowledge the financial support of the National Council for Scientific and Technological Development (CNPq), the Coordination for the Improvement of Higher Education Personnel (CAPES/PROEX) – Brazil and Bruning Tecnometal Ltda. for providing materials, access to infrastructure, and technical discussions that supported the underlying research. The authors also acknowledge EMBRAER for technical discussions and contributions related to the application context of this study.

AUTHOR'S CONTRIBUTION STATEMENT

Conceptualization, E.L.S., M.G.L., L.L., A.P.O. and D.J.R.P.; Methodology, E.L.S., M.G.L., L.L., A.P.O. and D.J.R.P.; Formal Analysis, E.L.S. and M.G.L.; Investigation, E.L.S. and M.G.L.; Resources, E.L.S. and D.T.A.; Writing – Original Draft Preparation, E.L.S. and M.G.L.; Writing – Review & Editing, E.L.S. and D.T.A.; Visualization, E.L.S. and M.G.L.; Supervision, E.L.S. and D.T.A.

CONFLICTS OF INTEREST STATEMENT

L.L., D.T.A., A.P.O. and D.J.R.P. are employees of Bruning Tecnometal Ltda. The role of Bruning Tecnometal in the underlying research is described in the Author Contributions and Acknowledgments sections. The other authors declare that they have no known competing financial interests or personal relationships that could have appeared to influence the work reported in this paper.

REFERENCES

[1] Chen F.K., Huang T.B. Formability of stamping magnesium-alloy AZ31 sheets. Journal of Materials Processing Technology, 2003. https://doi.org/10.1016/S0924-0136(03)00684-8

[2] Wang Y.N., Huang J.C. Texture analysis in hexagonal materials. Materials Chemistry and Physics, 2003. https://doi.org/10.1016/S0254-0584(03)00168-8

[3] Barnett M.R., Ghaderi A., Quinta da Fonseca J., Robson J.D. Influence of orientation on twin nucleation and growth at low strains in a magnesium alloy. Acta Materialia, 2014. https://doi.org/10.1016/j.actamat.2014.07.013

[4] Shah S.S.A., Liu M., Khan A., Ahmad F., Abdullah M.R., Zhang X., Xu S., Peng Z. Twinning aspects and their efficient roles in wrought Mg alloys: a comprehensive review. Journal of Magnesium and Alloys, 2024; 12: 2201-2230. https://doi.org/10.1016/j.jma.2024.04.035

[5] Zhang K. *et al*. Experimental investigation of the viscoplastic behaviours and microstructure evolutions of AZ31B and Elektron 717 Mg-alloys. Materials & Design, 2019. https://doi.org/10.1016/j.matdes.2019.108160

[6] Bohlen J. *et al*. Processing Effects on the Formability of Magnesium Alloy Sheets. Metals, 2018. https://doi.org/10.3390/met8020147

[7] Stutz L. *et al*. Formability of Magnesium Sheet ZE10 and AZ31 with Respect to Initial Texture. Magnesium Technology 2016. https://doi.org/10.1007/978-3-319-48099-2_57

[8] Luo A.A., Shi R., Miao J., Avey T. Magnesium Shee*t al*loy Development for Room Temperature Forming. JOM, 2021; 73(5): 1403-1418. https://doi.org/10.1007/s11837-021-04616-y

[9] Luxfer Magnesium Rolled Products. Elektron 717 Highly Formable Magnesium Sheet. Technical datasheet.

[10] Schneider E.L. *et al*. Mechanical property evolution of ZE10A alloy subjected to thermomechanical treatments between 250 and 300 °C. Journal of Materials Research and Technology, 2025. https://doi.org/10.2139/ssrn.5387941

[11] Richter K. *et al*. Tempered forming of magnesium alloys using the example of roll forming. Materials Today: Proceedings, 2015. https://doi.org/10.1016/j.matpr.2015.05.018

[12] Silva B.C.S. *et al*. Tribological Investigations on Tool Surfaces for Temperature-Supported Forming of Magnesium AZ31 Sheets. Materials, 2020.

[13] Xu S., Xiao P., Wu X., Holmes J., Mompiou F., Xiao Z., Jin C., Li T., Wang K., Zeng Z. Mechanistic investigation of highly bendable magnesium alloy sheet fabricated by short-process manufacturing. Journal of Magnesium and Alloys, 2024; 12: 4289-4310. https://doi.org/10.1016/j.jma.2023.09.026

[14] Paisarn R., Yugi N., Koga N. Air bending of AZ31 magnesium alloy sheets. Journal of the Japan Institute of Light Metals, 2005; 55(4): 181-185. https://doi.org/10.2464/jilm.55.181

[15] Habibnejad-Korayem M. *et al*. Microstructure modification and bendability improvement of AZ31 magnesium sheet by bending-unbending and annealing. Materials Science and Engineering: A, 2015. https://doi.org/10.1016/j.msea.2015.09.047

[16] Wang L. *et al*. Evolution of springback and neutral layer of AZ31B magnesium alloy V-bending under warm forming conditions. Journal of Materials Processing Technology, 2013. https://doi.org/10.1016/j.jmatprotec.2013.01.005

[17] Wang H. *et al*. Finite Element Simulation and Experimental Study of U-Bending Forming of High-Strength Mg-Gd-Y-Zn-Zr Alloy. Metals, 2023. https://doi.org/10.3390/met13081477

[18] Okayasu M., Takeuchi S., Ohfuji H. Formability Improvement for Bending Magnesium Alloy AZ31 Sheet via Microstructural Control. Journal of Materials Engineering and Performance, 2025. https://doi.org/10.1007/s11665-024-09822-8

[19] Weiss M. *et al*. The Effect of the Forming Mode on Twinning and Springback in the Bending-Dominated Forming of Magnesium AZ31 Sheet. Metals, 2024. https://doi.org/10.3390/met14090983

[20] Kuo C.C., Lin B.T. Optimization of springback for AZ31 magnesium alloy sheets in the L-bending process based on the Taguchi method. The International Journal of Advanced Manufacturing Technology, 2012. https://doi.org/10.1007/s00170-011-3373-8

[21] Wang Y. *et al*. Tension-compression asymmetry and corresponding deformation mechanism in ZA21 magnesium

bars with bimodal structure. International Journal of Minerals, Metallurgy and Materials, 2023. https://doi.org/10.1007/s12613-021-2388-x

[22] Rustom S. *et al*. Manufacturing Strategies to Mitigate Deformation Twinning in Magnesium. ASME Open Journal of Engineering, 2023. https://doi.org/10.1115/1.4056553

[23] Ambrogio G. *et al*. Some considerations on force trends in incremental forming of different materials. Journal of Materials Processing Technology, 2005.

[24] Siddiqi M.U.R., Corney J.R., Sivaswamy G., Amir M., Bhattacharya R. Design and validation of a fixture for positive incremental sheet forming. Proceedings of the Institution of Mechanical Engineers, Part B: Journal of Engineering Manufacture, 2018; 232(4): 629-643. https://doi.org/10.1177/0954405417703423

[25] Hoefnagels J.P.M. *et al*. A Small-Scale, Contactless, Pure Bending Device for In-situ Electron Microscopy Testing. Experimental Mechanics, 2015. https://doi.org/10.1007/s11340-015-0046-9

[26] ASTM E290. Standard Test Methods for Bend Testing of Material for Ductility. ASTM International.

[27] ISO 7438. Metallic materials — Bend test. International Organization for Standardization.

[28] Fluke Corporation. Ti9, Ti10, Ti25, TiRx, TiR and TiR1 Thermal Imagers: User Manual. Rev. 2, 2010.

[29] Polimold Industrial S.A. Polimold MS (Mini Smart) Temperature Controller. Technical brochure.

https://doi.org/10.31875/2410-4701.2026.13.06